

Study of the reaction $\gamma p \rightarrow p\pi^0\eta$

The CB-ELSA Collaboration

I. Horn¹, A.V. Anisovich^{1,2}, G. Anton³, R. Bantes⁴, O. Bartholomy¹, R. Beck¹, Y. Beloglazov², R. Bogendörfer³, R. Castelijns⁵, V. Credé⁶, A. Ehmanns¹, J. Ernst¹, I. Fabry¹, H. Flemming^{7,a}, A. Fösel³, M. Fuchs¹, Ch. Funke¹, R. Gothe^{4,b}, A. Gridnev², E. Gutz¹, S. Höffgen⁴, J. Höbl³, J. Junkersfeld¹, H. Kalinowsky¹, F. Klein⁴, E. Klempt¹, H. Koch⁷, M. Konrad⁴, B. Kopf⁷, B. Krusche⁸, J. Langheinrich^{4,b}, H. Löhner⁵, I. Lopatin², J. Lotz¹, H. Matthäy⁷, D. Menze⁴, J. Messchendorp^{9,c}, V. Metag⁹, V.A. Nikonov^{1,2}, D. Novinski², M. Ostrick^{4,d}, H. van Pee¹, A. Radkov², A.V. Sarantsev^{1,2}, C. Schmidt¹, H. Schmieden⁴, B. Schoch⁴, G. Suft³, V. Sumachev², T. Szczepanek¹, U. Thoma¹, D. Walther¹, and Ch. Weinheimer^{1,e}

¹ Helmholtz-Institut für Strahlen- und Kernphysik, Universität Bonn, Germany

² Petersburg Nuclear Physics Institute, Gatchina, Russia

³ Physikalisches Institut, Universität Erlangen, Germany

⁴ Physikalisches Institut, Universität Bonn, Germany

⁵ Kernfysisch Versneller Instituut, Groningen, The Netherlands

⁶ Department of Physics, Florida State University, Tallahassee, FL, USA

⁷ Institut für Experimentalphysik I, Universität Bochum, Germany

⁸ Institut für Physik, Universität Basel, Switzerland

⁹ II. Physikalisches Institut, Universität Gießen, Germany

^a Present address: GSI, Darmstadt, Germany

^b Present address: University of South Carolina, Columbia, SC, USA

^c Present address: Kernfysisch Versneller Instituut, Groningen, The Netherlands

^d Present address: Institut für Kernphysik, Universität Mainz, Germany

^e Present address: Institut für Kernphysik, Universität Münster, Germany

Received: August 15, 2019/ Revised version:

Abstract. The reaction $\gamma p \rightarrow p\pi^0\eta$ has been studied with the CBELSA detector at the tagged photon beam of the Bonn electron stretcher facility. The reaction shows contributions from $\Delta^+(1232)\eta$, $N(1535)^+\pi^0$ and $pa_0(980)$ as intermediate states. A partial wave analysis suggests that the reaction proceeds via formation of six Δ resonances, $\Delta(1600)P_{33}$, $\Delta(1920)P_{33}$, $\Delta(1700)D_{33}$, $\Delta(1940)D_{33}$, $\Delta(1905)F_{35}$, $\Delta(2360)D_{33}$, and two nucleon resonances $N(1880)P_{11}$ and $N(2200)P_{13}$, for which pole positions and decay branching ratios are given.

PACS: 13.30.-a Decays of baryons, 13.60.Le Meson production 14.20.Gk Baryon resonances with $S = 0$

1 Introduction

The study of baryon resonances has found renewed interest as evidenced by new experimental facilities providing continuous photon beams like Jefferson Lab, SPring-8, MAMI at Mainz, and ELSA at Bonn. For nucleon resonances up to $\approx 1.7 \text{ GeV}/c^2$, their abundance and most masses are reasonably well explained in quark models even though the models use very different assumptions on the nature of long-range quark-quark interactions, like effective gluon exchange [1], instanton induced interactions [2], or exchange of Goldstone bosons [3]. At higher masses, the models differ in important details of their predictions but agree in predicting the existence of many more states than

have been found experimentally. Diquark models [4] have a reduced number of degrees of freedom and expect fewer states [5,6]. Models based on a conformal approximation of QCD exploit the correspondence [7] between string theories on an Anti-de-Sitter (AdS) space and gauge theories on its space-time boundary [8,9]. Apparently, AdS/QCD predicts a smaller number of states [10,11,12,13] but, to our knowledge, the problem of *missing resonances*, of resonances predicted in quark models but not in AdS/QCD, has not yet been discussed. Lattice gauge calculations aim at simulating full QCD; substantial progress has been achieved [14], however, the calculations do not yet help to validate or reject specific quark models.

In the past, knowledge on nucleon resonances was derived mostly from partial wave analyses of elastic πN scattering experiments. This method exploits the coupling

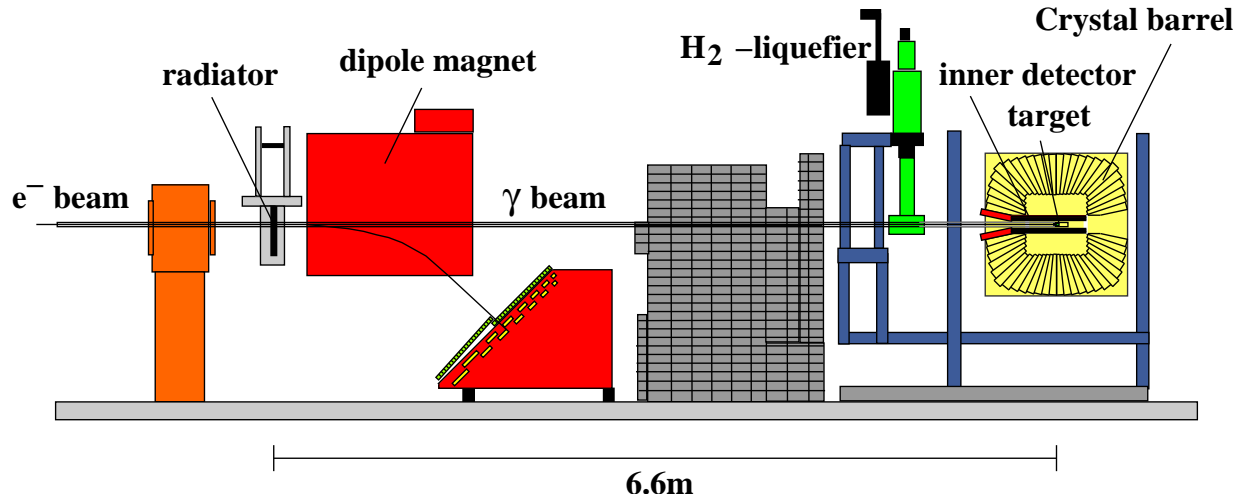


Fig. 1. Experimental setup at ELSA in Bonn: Electrons delivered by the accelerator ELSA enter the experimental area from the left. They hit a radiator and produce a wide-band photon beam. The photon energy is tagged by measuring the electron deflecting angle in a dipole magnet. The photons hit protons of a liquid H_2 target. Particles, in particular photons, emerging from the reaction are detected in the Crystal barrel detector. A scintillation fiber (scifi) detector measures the direction of charged particles. A total absorption lead mineral oil Čerenkov counter installed further downstream to monitor the photon beam intensity is not shown in the figure.

of resonances to the $N\pi$ channel; resonances for which this coupling is weak are not detectable. The Particle Data Listings [15] teach us that at high pion momenta, above 2 GeV, high-spin states are formed while formation of high-mass states with low angular momenta seems to be suppressed. Due to this limitation, only few resonances are known so far. Even worse, the evidence for a large fraction of them has recently been questioned in a careful analysis [16] of a large body of $N\pi$ elastic and charge-exchange scattering data.

The new facilities give access to photo-induced production of resonances; detectors with large solid angle allow one to study decays of resonances into complex final states. Thus $N\pi$ is avoided in the entrance and in the exit channel. Quark model calculations [17] and first results [18,19] seem to support our conjecture that in photoproduction, excitation of radially excited states might be preferred over excitations of high-angular momentum states.

In this paper we present a study of the reaction

$$\gamma p \rightarrow p\pi^0\eta \quad (1)$$

for photon energies covering the resonance region from the $p\pi^0\eta$ production threshold at $W = 1.63 \text{ GeV}/c^2$ up to $2.5 \text{ GeV}/c^2$. In this reaction, decays of Δ resonances into $\Delta(1232)\eta$ can be studied: the η acts as an isospin filter and resonances decaying into $\Delta(1232)\eta$ must have isospin $I = 3/2$. For low photon energies phase space is limited, and $\Delta(1232)$ and η should be in a relative S-wave. We thus may expect a high sensitivity for baryon resonances with isospin $I = 3/2$ and spin $J = 3/2$ and negative parity. If such resonances decay into $N\pi$, they need $L = 2$ between N and π ; resonances with these quantum numbers

are characterized by $L_{2I,2J} = D_{33}$. The lowest mass resonance with these quantum numbers is $\Delta(1700)D_{33}$. The possibility that it may couple to the $\Delta(1232)\eta$ channel was already discussed by Nefkens [20]; his conjecture was confirmed recently by the GRAAL collaboration [21]. The aim of this paper is to report evidence for Δ resonances above $\Delta(1700)D_{33}$, in particular for a $J^P = 3/2^\pm$ parity doublet consisting of the two resonances $\Delta(1920)P_{33}$ and $\Delta(1940)D_{33}$.

2 Experimental setup and data reconstruction

The experiment was carried out at the tagged photon beam of the **E**lectron **S**tretcher **A**ccelerator ELSA at Bonn [22], using the Crystal Barrel detector [23]. A short description of the experiment, data reconstruction and analysis methods can be found in a recent letter on $2\pi^0$ photoproduction [24]; further details are given in [25]. A schematic drawing of the experimental setup is shown in Fig. 1. For the data presented here, ELSA delivered - via slow extraction - a continuous electron beam of 3.2 GeV. The electrons hit a radiator target of $0.003 X_R$ (i.e. radiation length) thickness.

The energies of photons produced in the radiator target were tagged in energy by a measurement of the deflection angle of scattered electrons passing the field of a dipole magnet. For singly scattered electrons, the photon energy is $E_\gamma = E_0 - E_{e^-}$. The tagging detector consisted of 2 Multi-Wire Proportional Chambers (MWPCs) and 14 plastic scintillator bars. The position resolution of the MWPCs determined the photon energy resolution of 0.5 MeV at the highest E_γ and 30 MeV at the lowest E_γ , whereas the scintillation counters enabled fast timing. The

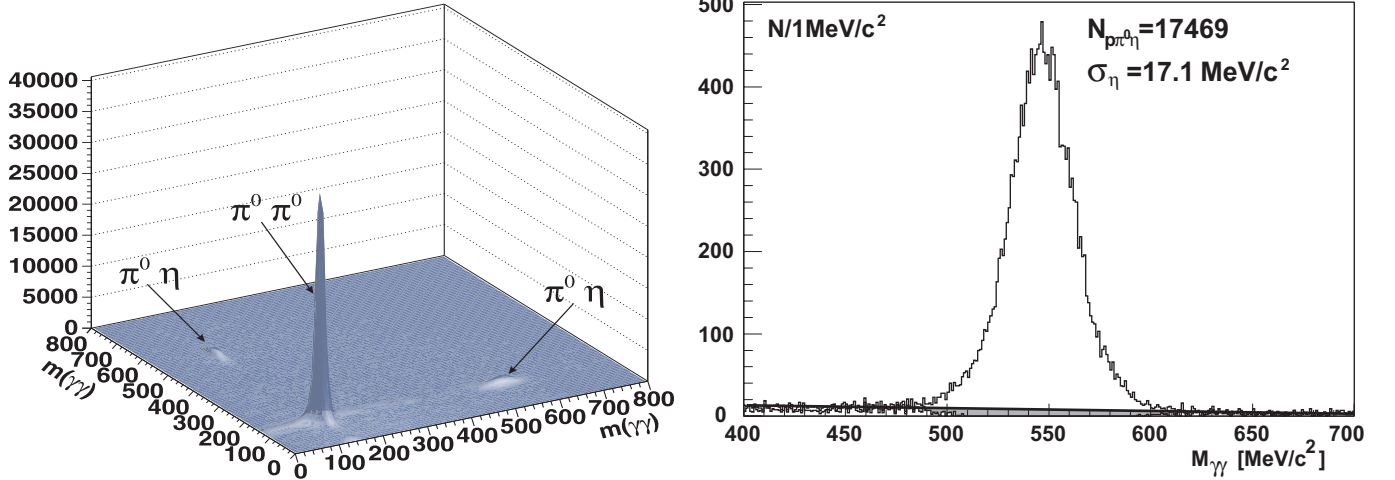


Fig. 2. Left: The distribution of $\gamma\gamma$ invariant masses after a kinematic fit to $\gamma p \rightarrow p4\gamma$ (with c.l.> 0.1%). There are six entries per event. The distribution shows a large peak due to the reaction $\gamma p \rightarrow p\pi^0\pi^0$ and two smaller peaks due to $\gamma p \rightarrow p\pi^0\eta$. Right: The $\gamma\gamma$ invariant mass distribution after a kinematic fit to $\gamma p \rightarrow p\pi^0\gamma\gamma$ (with c.l.> 10%) and a cut rejecting $\gamma p \rightarrow p\pi^0\pi^0$ events (with c.l.> 1%). In the 460-620 MeV/c² mass interval there are 18589 events, 1120 of them are below the background line derived from a linear fit. The fit to $\gamma p \rightarrow p\pi^0\eta$ (with c.l.> 1%) accepts 18379 events and rejects 210 background events leading to 910 background events (grey-shaded area).

energy calibration of the tagger was performed by direct injection of the electron beam.

The photon beam hit a liquid H₂ target (length: $l = 52.84$ mm, diameter: $d = 30$ mm); charged reaction products were detected in an inner three-layer scintillating-fiber detector surrounding the target and positioned at mean radii of 5.81 cm, 6.17 cm and 6.45 cm, respectively. The 2 mm fibers are partly bent to helical shapes (-25° , $+25^\circ$, 0° from the inner to the outer layer) to provide an unambiguous impact point when a charged particle crosses the detector [26].

The Crystal-Barrel calorimeter consisted of 1380 16-radiation-length CsI(Tl) crystals. The crystals are of trapezoidal shape and point to the center of the target; they provide an excellent photon detection efficiency and a high granularity. The setup covered about 98% of 4π (full ϕ coverage, $12^\circ \leq \theta \leq 168^\circ$). Its large solid-angle coverage allowed for reconstruction of multi-photon final states.

The first-level trigger was derived from a coincidence between the tagging system and the fiber detector. In the second-level trigger, a FAsT Cluster Encoder (FACE) based on cellular logic, provided the number of charged and neutral particles detected in the Crystal Barrel. Data were taken triggering on events with two (partly three) or more particles in the cluster logic. A segmented total-absorption oil Čerenkov counter determined the total photon flux.

Events due to reaction (1) were selected by requiring five clusters of energy deposits in the Crystal Barrel calorimeter. One of the clusters was required to match with the charged particle emerging from the liquid H₂ target and hitting the scintillation fiber detector. The latter cluster was identified as proton, the other four as photons. The proton and the four photons were assumed to

be produced in the target center. More details on event reconstruction can be found in [25].

These events were subjected to a kinematic fit to the $\gamma p \rightarrow p4\gamma$ hypothesis imposing energy and momentum conservation. The distribution of the $\gamma\gamma$ invariant mass of one pair against the second pair of surviving events (with 6 entries per event) is shown in Fig. 2, left panel. Then, the $\gamma p \rightarrow p\pi^0\gamma\gamma$ hypothesis was tested and events with a confidence level (c.l.) exceeding 10% were retained. In a next step, events compatible at a c.l. > 1% with the $\gamma p \rightarrow p2\pi^0$ hypothesis were rejected. The resulting $\gamma\gamma$ invariant mass of the second photon-pair is shown in Fig. 2, right panel. These events passed a final kinematic fit to the $\gamma p \rightarrow p\pi^0\eta$ hypothesis requiring a probability exceeding 1%. The final event sample contains 17469 events due to reaction (1) and 910 background events. Events which are likely due to the background are identified (and subtracted) by selecting those 910 events which are closest in phase space to the events falling into the η side bins (380-440 MeV/c²; 640-700 MeV/c²).

3 Mass and angular distributions

Fig. 3 shows a series of $p\pi^0\eta$ Dalitz plots for $M^2(p\eta)$ and $M^2(\pi^0\eta)$ versus $M^2(p\pi^0)$ restricted to slices in the γp invariant mass W , with W covering the threshold region (a) $1.7 < W < 1.9$ GeV/c², (b) for $1.9 < W < 2.05$ GeV/c², (c) $2.05 < W < 2.25$ GeV/c², and (d) $2.25 < W < 2.5$ GeV/c². Figs. (e) and (f) show Dalitz plots for $M^2(\pi\eta)$ versus $M^2(p\pi^0)$ for the highest energy bin. The figures in the lower part, (g) to (l), show the same Dalitz plots as above but calculated from the partial wave fit. All significant structures in the Dalitz plots are reasonably well reproduced. At low energies, for $W < 2.05$ GeV/c², the

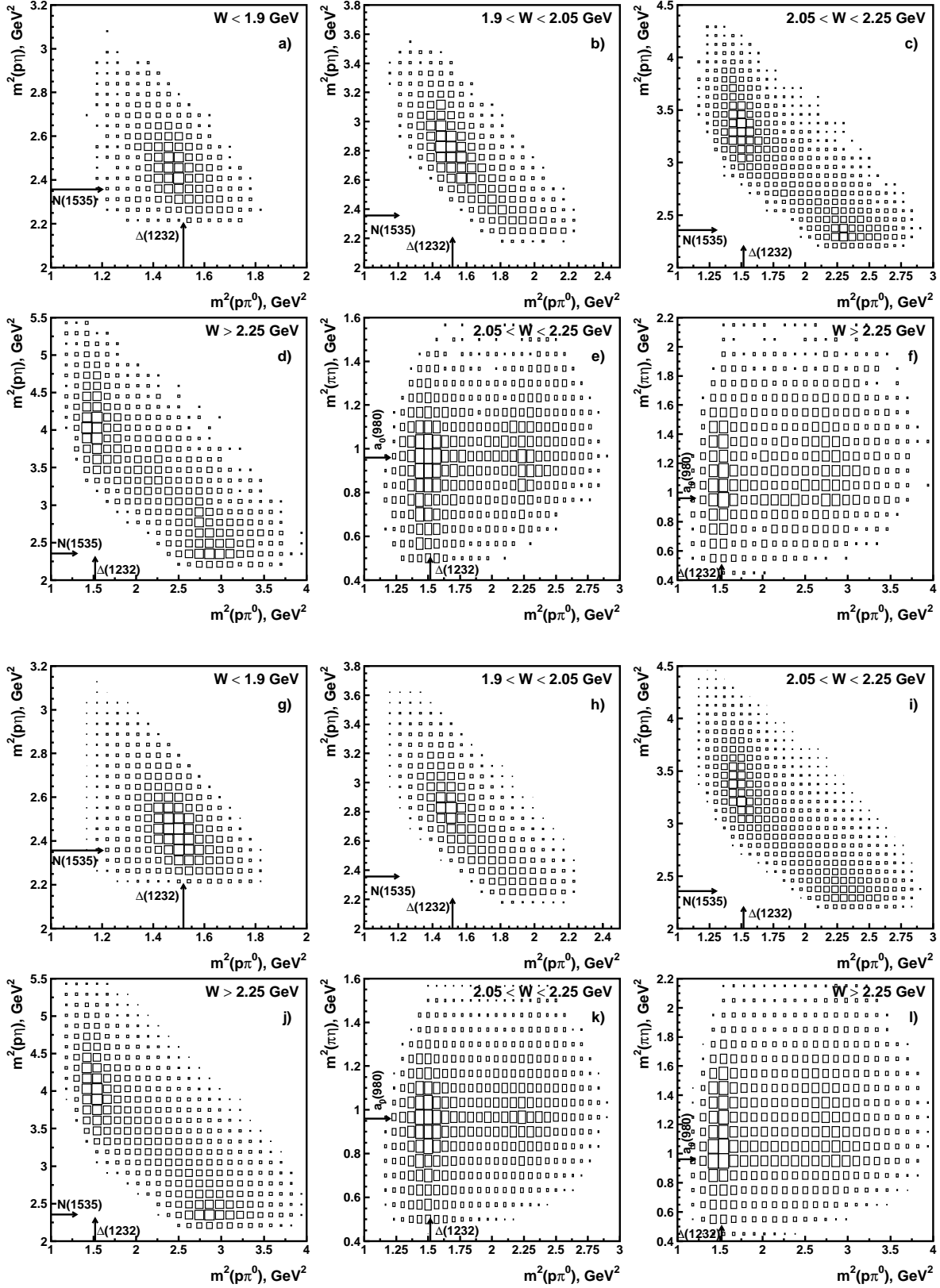


Fig. 3. Dalitz plot for the reaction $\gamma p \rightarrow p\pi^0\eta$ for various ranges of the total energy, data (a-f). The plots (a-d) show $M^2(p\eta)$ versus $M^2(p\pi^0)$, (e,f) $M^2(\pi^0\eta)$ versus $M^2(p\pi^0)$. With increasing energy, $\Delta(1232)\eta$ and $N(1535)\pi$ production fill different kinematical regions and are well separated. $N(1535)\pi$ is visible only for high photon energies even though the $N(1535)\pi$ production threshold (~ 1.0 GeV) is lower than the $\Delta(1232)\eta$ production threshold (~ 1.2 GeV). The lower part (g-f) show results of the event-based likelihood fit.

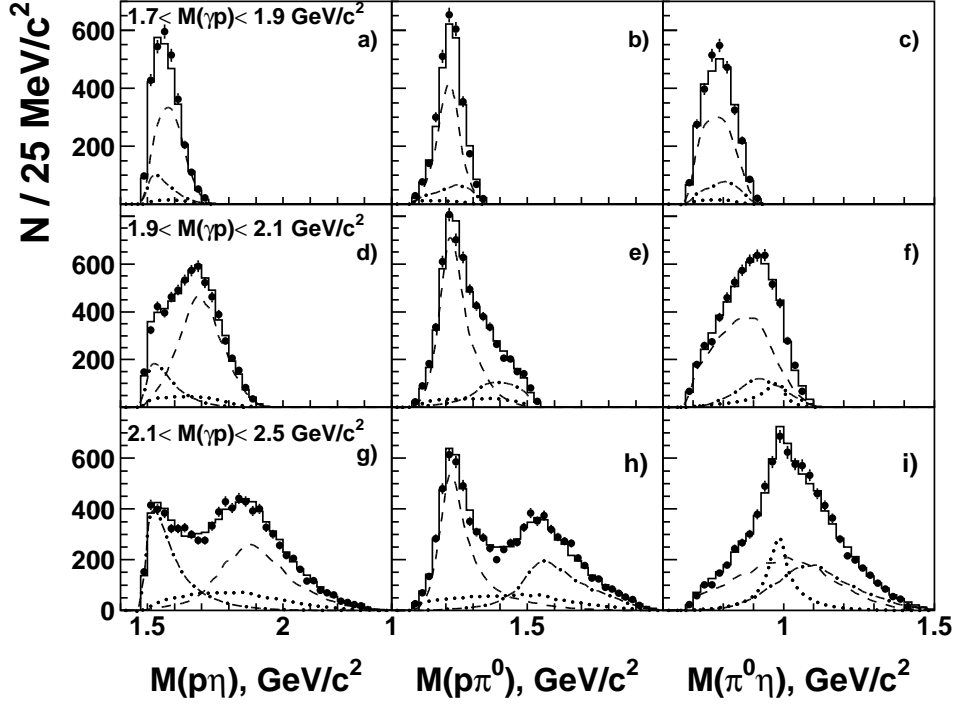


Fig. 4. Mass distributions for three values of $W = M(\gamma p)$. Data are represented by dots. The distributions are not corrected for the detector acceptance; errors are of statistical nature only. The solid curves show the result of the best fit. The dashed line stands for the $\Delta(1232)\eta$, the dashed-dotted line for the $N(1535)S_{11}\pi$, and the dotted line for the $p_{a_0}(980)$ partial wave contribution as determined in the partial wave analysis.

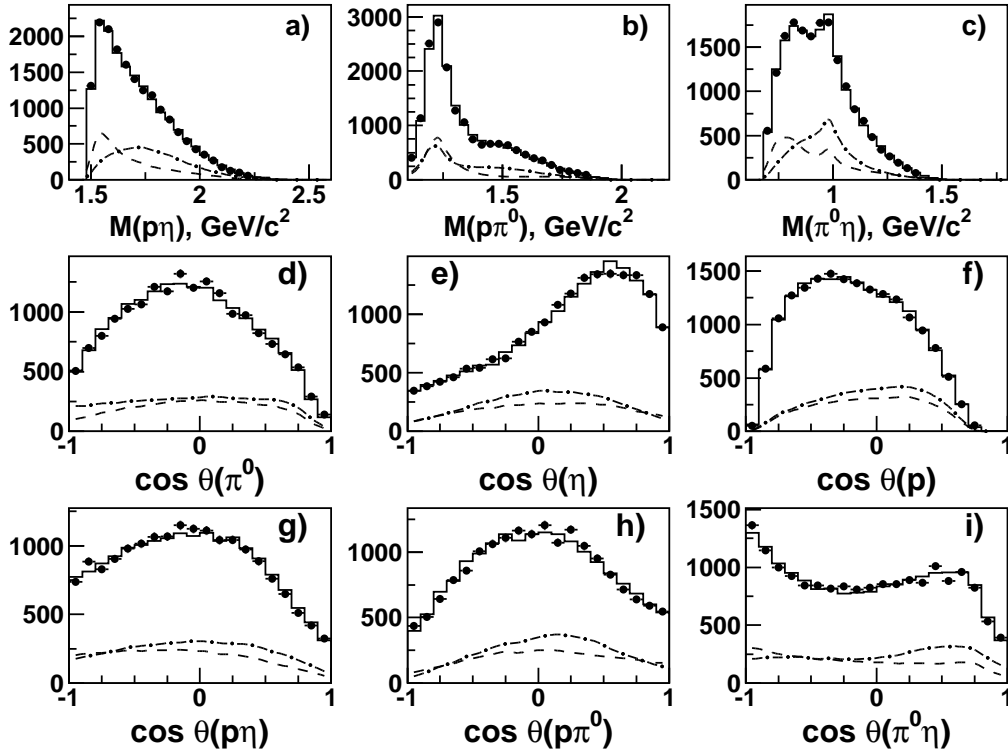


Fig. 5. Mass and angular distributions for the full data set. The distributions are not corrected for acceptance to allow a fair comparison of the fit with the data without introducing any model dependence by extrapolating e.g. over acceptance holes. Data are represented by dots, the fit as solid line. Errors are of statistical nature only. The dashed line stands for the D_{33} , the dashed-dotted line for the P_{33} partial wave contribution. There are further PWA contributions which are not shown. In (d-f), θ is the angle of a π^0 (d), η (e), p (f) with respect to the incoming photon in the center-of-mass-system (cms); in (g) the angle between the η and π^0 in the $p\eta$ rest frame, in (h) the angle between π^0 and η in the $p\pi^0$ rest frame, and in (i), the angle between π^0 and p in the $\pi^0\eta$ rest frame.

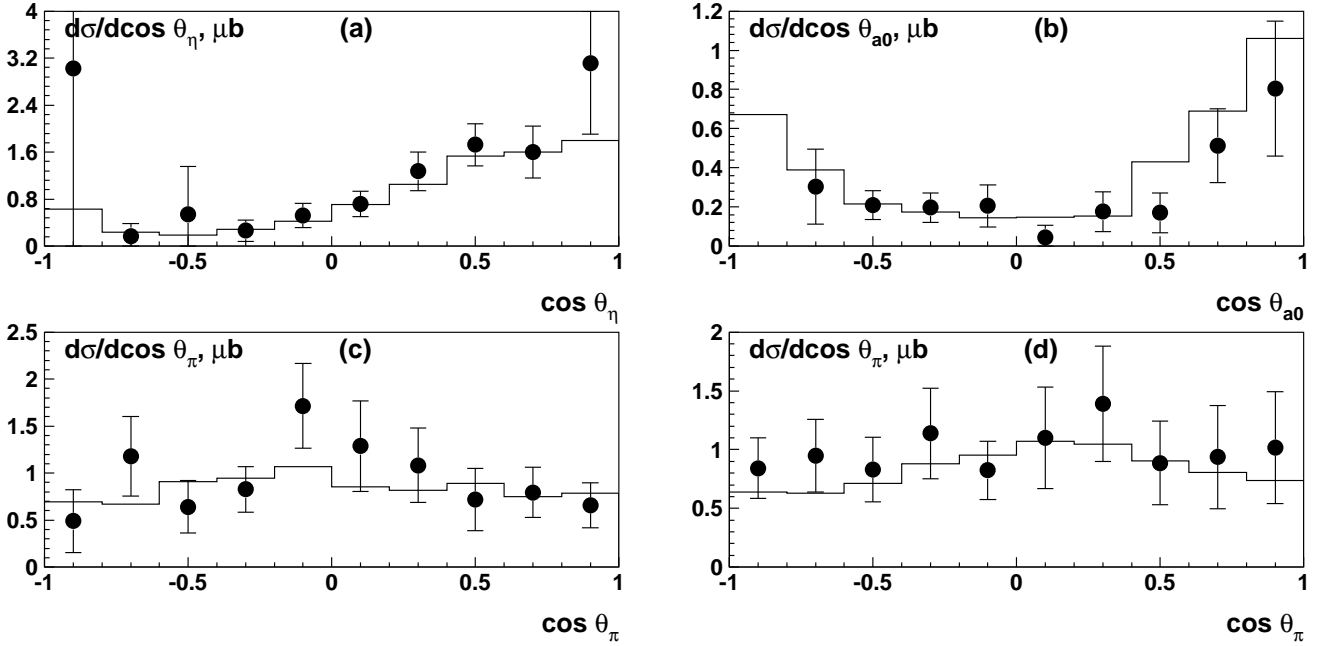


Fig. 6. a: Angular distribution of η with respect to the photon direction in the γp center-of-mass system. b: Center-of-mass angular distribution of $a_0(980)$ recoiling against the proton with respect to the photon beam axis for $E_\gamma > 2.0$ GeV. c and d: Angular distribution of pions recoiling in the helicity (c) and Godfrey Jackson (d) frame (after side bin subtraction). The latter two distributions are presented for $1.9 < E_\gamma < 2$ GeV and $1.15 < M_{p\pi} < 1.30$ to select $\Delta\eta$ decays, the cuts $1.075 < M_{p\pi} < 1.150$ and $1.300 < M_{p\pi} < 1.375$ GeV/ c^2 define the side bins. Losses due to the cuts are corrected using Monte Carlo simulations (see text). The energy region contains large contributions from $\Delta(1920)P_{33}$ and $\Delta(1940)D_{33}$. In all four sub-figures, dots with error bars give data, the histogram represents the PWA fit.

Dalitz plots are dominated by $\Delta(1232)\eta$; at high energies, the $N(1535)\pi$ intermediate state is observed. Under these kinematical conditions, the two contributions populate different kinematical regions and can be separated easily. The early onset of $\Delta(1232)\eta$ is, at the first glance, surprising since the threshold for $\Delta(1232)\eta$ is higher than for $N(1535)\pi$ production. Within the partial wave analysis this is explained by contributions from $\Delta(1700)D_{33}$ and $\Delta(1600)P_{33}$. The two resonances can be produced by an electric or magnetic dipole transition (and higher-order transitions), respectively, and decay in $\Delta(1232)\eta$ via S- or P-wave while decays into $N(1535)\pi$ require P- and D-waves.

Three different 2-body invariant masses can be formed in reaction (1), the $p\eta$, $p\pi^0$, and $\pi^0\eta$ mass distributions. They are shown in Fig. 4 for three ranges of photon energies. The distributions undergo significant changes when the photon energy is varied. In the threshold region, ($1.7 \leq W \leq 1.9$ GeV/ c^2), the $p\pi^0$ invariant mass distribution (Fig. 4b) suggests a significant $\Delta(1232)$ contribution (a presumption confirmed in the partial wave analysis), the $p\eta$ (Fig. 4a) and $\pi^0\eta$ (Fig. 4c) mass distributions show no significant structures. In the 1.9 to 2.1 GeV/ c^2 mass region, $\Delta(1232)\eta$ is still significant, a small $p\eta$ threshold effect is observed (Fig. 4d). Above 2.1 GeV/ c^2 , $N(1535)\pi$ – with $N(1535)$ decaying into $N\eta$ – becomes visible (Fig. 4g). At these energies, $N(1535)$ production is significant and comparable in intensity to the $\Delta(1232)$. In the $\pi^0\eta$ mass distribution, a peak is observed at 1 GeV/ c^2 (Fig.

4i) which we assign to the $pa_0(980)$ intermediate state. Mass projections for the full data set and some angular distributions are presented in Fig. 5. The P_{33} and D_{33} partial wave contribution are also shown.

We now turn to the discussion of a few specific angular distributions. In the threshold region for $p\pi^0\eta$ photoproduction we may expect S- and P-waves to dominate the decay mode. S-wave decays into $\Delta(1232)\eta$ require D_{33} quantum numbers which can be reached by an electric dipole transitions; magnetic dipole transitions lead to P_{33} quantum numbers for which P-wave decays into $\Delta(1232)\eta$ are possible. If one of the two amplitudes prevails, we may expect an isotropic angular distribution for the recoiling pion. In case of both amplitudes being present, S-P interference leads to a linear increase with $\cos\theta_\eta$, a distribution which is clearly contributing to the data (Fig. 6a).

At the largest photon energies, a peak due to $a_0(980)$ production can be identified in the $\pi\eta$ invariant mass distribution. In Fig. 6b the $a_0(980)$ angular distribution with respect to the photon beam is presented (after side bin subtraction). The $a_0(980)$ signal region is defined by $0.96 < M_{\pi\eta} < 1.04$ GeV/ c^2 , the sidebins with $0.88 < M_{\pi\eta} < 0.96$ and $1.04 < M_{\pi\eta} < 1.12$ are subtracted with weight 1/2. The side bin subtraction suffers from the large $a_0(980)$ width, hence the distribution must be viewed with some precaution. However, it agrees reasonably well with the PWA result and the subtraction is justified a posteriori.

Surprisingly, $a_0(980)$ is not mostly produced in forward direction as might be expected if the main $a_0(980)$ produc-

tion mechanism would have been vector-meson exchange in the t -channel (exploiting a $a_0(980) \rightarrow \gamma \rho/\omega$ coupling). A significant fraction of the $a_0(980)$ signal seems to stem from the decay of high-mass resonances. This suspicion is supported by the partial wave analysis.

Fig. 6c and d show $\Delta(1232) \rightarrow p\pi^0$ decay angular distributions which should reflect the spin $J = 3/2^+$ quantum numbers of $\Delta(1232)$. The π^0 angular distribution from Δ decays is shown as pion emission angle with respect to the Δ flight direction (helicity frame, Fig. 6c), or with respect to the photon beam direction (Godfrey-Jackson frame, Fig. 6d). The photon energy is restricted to $W < 1.9 \text{ GeV}/c^2$. The distributions are essentially flat (preventing a straightforward identification of the $\Delta(1232)$ spin) indicating that $\Delta(1232)$ are likely not produced by one helicity amplitude only and in a single reaction chain. Explicit expressions for typical angular distributions are given elsewhere [28].

4 Partial wave analysis

4.1 The method

The qualitative findings discussed in the previous section are confirmed in a partial wave analysis (PWA). The formalism is documented in [27, 28, 29]. In addition to the data presented here, data on photoproduction of single pions, η 's, and of Λ and Σ hyperons are included as well as some important partial-wave amplitudes for πN elastic scattering. References to the data, an outline of the PWA method and the definition of total likelihood and likelihood contributions can be found in [30]. The different data sets entered with appropriately chosen weights w_i ; the weights vary from 1 (for data which should be reproduced qualitatively) to 30 (for low-statistics data like polarization data which we insist to be well reproduced in the fits). The weights are given in Table 4 of [30]. The weights are chosen to ensure that there is good qualitative agreement between data and fit even for low-statistics data which otherwise may be dominated by the influence of high-statistics data. The mean weight is $\bar{w} = 4.2$. For this data, $w_{\gamma p \rightarrow p\pi^0\eta} = 10$ was chosen; (much) smaller weights lead to discrepancies between fit and this data, higher weights deteriorate the fits elsewhere. We minimized a pseudo-log-likelihood function $\ln \mathcal{L}_{\text{tot}}$ defined as a sum of the log-likelihoods of fits to $\gamma p \rightarrow \pi^0\pi^0$ and $\gamma p \rightarrow \pi^0\eta$, and of the $\chi^2/2$ contributions of all data given in the form of histograms.

The $\gamma p \rightarrow p\pi^0\pi^0$ and $\gamma p \rightarrow p\pi^0\eta$ data are fitted using an event-based maximum likelihood method which takes into account the full correlations between all variables in the 5-dimensional phase space. New data on the beam asymmetry Σ for $\gamma p \rightarrow p\pi^0\eta$ [31] were included in the partial wave analysis. Since the prediction for Σ were already close to the data [32], the new data on Σ did not change the PWA results.

As a starting point, we used the set of resonances of [30] and added resonances in the partial waves listed in Table 1. The Table gives the quantum numbers of baryon

Table 1. The lowest partial waves which may contribute to $\gamma p \rightarrow p\pi\eta$.

L	$\Delta(1232)\eta$	$N(1535)\pi$	$pa_0(980)$
0	D_{33}	P_{11}, P_{31}	P_{11}, P_{31}
1	P_{31}, P_{33}, F_{35}	$S_{11}, D_{13}, S_{31}, D_{33}$	$S_{11}, D_{13}, S_{31}, D_{33}$
2	$S_{31}, D_{33}, D_{35}, G_{37}$	$P_{13}, F_{15}, P_{33}, F_{35}$	$P_{13}, F_{15}, P_{33}, F_{35}$

resonances which could contribute to the $p\pi\eta$ final state assuming that the relative orbital angular momenta between meson and baryon in the three visible intermediate states $\Delta(1232)\eta$, $N(1535)\pi$, and $pa_0(980)$ are restricted to $L \leq 2$. First, resonances of the first line were tested but their decays with $L = 1$ and $L = 2$ were also admitted. It turned out that for nearly all resonances, inclusion of $L = 2$ decays led to marginal likelihood improvements ($\Delta \ln \mathcal{L}_{\pi^0\eta} < 5$ corresponding to a statistical significance of less than two standard deviations. The $\Delta(1232)\eta$ D-wave contribution, e.g., was found to be negligible for $\Delta(1700)D_{33}$, below 1% for $\Delta(1940)D_{33}$ while for $\Delta(2360)D_{33}$, the S and D wave couplings had similar magnitudes. The partial waves in the second (and third) line of Table 1 were tested one by one. No significant contribution was found except for a small fraction of $\Delta(1905)F_{35}$ in its $\Delta(1232)\eta$ decay. Its fraction in $N(1535)\pi$ (with $L = 2$) is marginal.

The quality of the final PWA fit to the data is shown in Fig. 4 and 5. In the latter figure, the full statistics integrated over the full energy range is shown; the agreement between data and fit result is very convincing and equally good when mass slices are selected or other variables are plotted. It has to be remembered that a likelihood fit uses the full kinematics of each event and that neither the Dalitz plots (Fig. 3) nor the projections (Fig. 4) are fitted.

4.2 Isospin considerations

Some resonances, even though known to exist, cannot be reasonably included in the partial wave analysis, for technical reasons. We need e.g. a $J^P = 1/2^+$ resonance at about $1900 \text{ MeV}/c^2$. A $N(1880)P_{11}$ resonance (formerly called $N(1840)$ by us [19]) is required to describe the two reactions $\gamma p \rightarrow \Lambda K^+$ and $\gamma p \rightarrow \Sigma K^+$ (which define the isospin of contributing resonances). Both, $N(1880)P_{11}$ and $\Delta(1910)P_{31}$, can decay into $N(1535)\pi$ and/or $pa_0(980)$, and there is no information in these two decay modes to decide on the isospin. Hence both might be present. The $\Delta(1910)P_{31}$ might decay into $\Delta(1232)\eta$ but this is not observed. Thus there is evidence for $N(1880)P_{11}$ and no direct evidence for an additional $\Delta(1910)P_{31}$. However, a $\Delta(1910)P_{31}$ might nevertheless exist and contribute to $p\pi^0\eta$ if it couples to $N(1535)\pi$ and/or $pa_0(980)$ but not to ΣK^+ and $\Delta(1232)\eta$ (or only with a weak coupling). In such a case (which admittedly is a bit constructed but

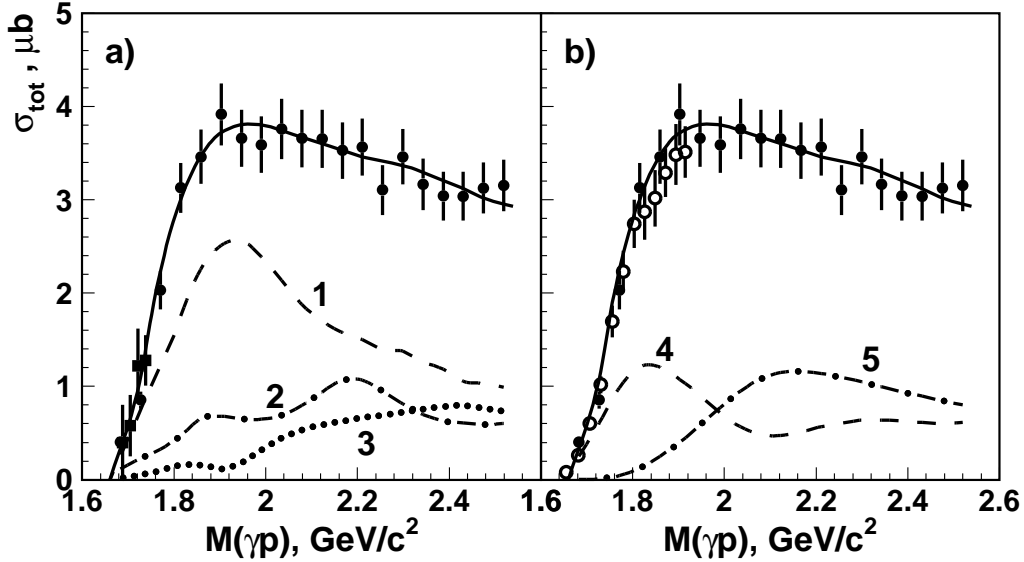


Fig. 7. Total cross sections for $\gamma p \rightarrow p\pi^0\eta$. In both panels, our data are represented by \bullet with error bars; the solid curves represents our PWA fit. Comparison to other data and two decompositions of the total cross sections are shown in two sub-figures. a) Our data compared to data from Nakabayashi *et al.* [33] \blacksquare . Curve 1 shows the cross section for $\gamma p \rightarrow \Delta(1232)\eta$, curve 2 that for $N(1535)\pi$, and curve 3 that for $\gamma p \rightarrow pa_0(980)$. These cross sections are not corrected for unseen decay modes. b) open circles: Ajaka *et al.* [21]. Partial wave decomposition of the cross section into the D_{33} (curve 4) and the P_{33} partial wave (curve 5).

not forbidden by any selection rule), $\Delta(1910)P_{31}$ decays into $p\pi^0\eta$ are discarded. The reason for this is that introduction of two close-by resonances in one final state having different isospin but otherwise identical quantum numbers leads very often to very large amplitudes for both resonances and destructive interference.

The $N(2200)P_{13}$ was introduced, too, in [19]. Here, it is found to contribute significantly to $p\pi^0\eta$ but not to $\Delta(1232)\eta$. Hence we assume it to belong to the family of nucleon resonances, and do not include a further $\Delta(2200)P_{33}$. For the same reason we do not allow $N(1875)D_{13}$ to decay into $N(1535)\pi$ and/or $pa_0(980)$; in the $3/2^-$ partial wave, the intensity in $p\pi^0\eta$ is assigned to $\Delta(1940)D_{33}$. The isospin $I = 3/2$ is identified from the $\Delta\eta$ decay mode. Contributions from $I = 1/2$ to $N(1535)\pi$ and/or $pa_0(980)$ are possible but are not considered here because of limitations of the data base. A separation of two isospin contributions would require a second isospin channel, e.g., the study of $\gamma p \rightarrow n\pi^+\eta$.

4.3 The total cross section

The final fit required contributions to the $p \rightarrow p\pi^0\eta$ final state from eight resonances; these are listed in Table 2. Two of them do not couple to $\Delta(1232)\eta$ and are interpreted as nucleon resonances. The $N(1880)$ could be the missing P_{11} resonance forming, jointly with $N(1900)P_{13}$, $N(2000)F_{15}$, $N(1990)F_{17}$, a super-multiplet with (dominantly) $L=2, S=3/2$. The $N(2200)P_{13}$ might be a $N(1900)P_{13}$ radial excitation.

In Fig. 7 the total cross section is displayed. The points with errors give the acceptance-corrected results of the measurement and their statistical and systematic errors but not the $\pm 15\%$ systematic error assigned to the photon-flux normalization. The solid curve shows the result of the partial wave analysis (PWA). The total cross section reaches the maximum of $4\mu b$ in the $2\text{ GeV}/c^2$ region and then decreases slowly to $3\mu b$. In the threshold region, our cross section is fully compatible with results obtained at Sendai [33]. The cross section determined by GRAAL [21] falls systematically below our values but the difference is covered by the 15% normalization error.

The acceptance is calculated using Monte Carlo techniques. The full apparatus is simulated using GEANT3. Detection and reconstruction efficiency, probabilities for split-offs for photons and charged particles, confidence level distributions for the different kinematical fits for real data and Monte Carlo data were compared carefully. The detector is well understood by the Monte Carlo simulation [25]. The mean acceptance for the $p4\gamma$ final state is 15-20% but the acceptance vanishes for forward protons escaping through the forward hole in the detector. Hence a proper extrapolation of the four-dimensional event distribution into the uncovered region of the detector is essential.

Table 2. Resonances used in the partial wave analysis.

$N(1880)P_{11}$	$N(2200)P_{13}$	$\Delta(1600)P_{33}$	$\Delta(1920)P_{33}$
$\Delta(1700)D_{33}$	$\Delta(1940)D_{33}$	$\Delta(2360)D_{33}$	$\Delta(1905)F_{35}$

For this purpose, phase space distributed events due reaction (1) were simulated according to the photon flux. These events were weighted with the PWA solution. The resulting event sample represents the ‘true’ physics, in the limit that data and partial wave analysis are correct. The curves in Figures 6 and 7 are calculated as Monte Carlo integral over this (weighted) event sample. The detection efficiency for the data is obtained from the ratio of reconstructed and generated events of the weighted Monte Carlo event sample.

The systematic error comprises the error in the reconstruction efficiency (5.7%) and a few small errors ($\approx 1\%$) due to uncertainties in target position and profile of the photon beam, and the extrapolation of the intensity distribution into blind regions of the detector (mainly for forward protons). The latter uncertainty is estimated to about 5% by using different PWA solutions giving acceptable descriptions of the data. These errors are added in quadrature and included in Fig. 7. The largest error stems from the uncertainty in the photon flux: the normalization derived from a comparison of the π^0 photoproduction cross section with SAID (see [25]). The normalization error of $\pm 15\%$ is not included.

The excitation functions for the three intermediate states $\Delta(1232)\eta$, $N(1535)\pi$, and $pa_0(980)$, deduced from the partial wave analysis, are shown in Fig. 7a. The $\Delta(1232)\eta$ makes the most significant contribution to the total cross section; at threshold, it dominates the reaction. It reaches a peak height just below $2\text{ GeV}/c^2$. The $N(1535)\pi$ intermediate state exhibits a structure at $1.9\text{ GeV}/c^2$ (due to the $N(1880)P_{11}$) and a second bump at $2.2\text{ GeV}/c^2$ which we interpret as $N(2200)P_{13}$. With increasing mass, $pa_0(980)$ gains a notable intensity. The excitation functions shown in Fig. 7 represent the best solution. It should be stressed that these contributions are qualitative; the numerical values differ significantly for different fits, much more than the pole positions of the contribution resonances. The errors in the excitation functions can be, in particular at high energies, as large as 30%.

4.4 Resonances contributing to $p\pi^0\eta$

In a first approach, we used Breit-Wigner resonances for less important waves while S_{11} , P_{11} , P_{13} , P_{33} , and D_{33} were described within the K-matrix/P-vector approach [30]. For these waves, elastic πN scattering amplitudes from [16] were included in these fits. For the two waves P_{33} and D_{33} discussed here, a satisfactory description was obtained with a 6-channel ($N\pi$, $\Delta(1232)\pi$ (S, D -waves for D_{33} and P, F -waves for P_{33}), $\Delta(1232)\eta$, $N(1535)\pi$, $N a_0(980)$) 3-pole parameterization. Parameterizations of the S_{11} , P_{11} , and P_{13} amplitudes are given in [29], those for P_{33} and D_{33} are presented in Tables 3 and 4.

All eight resonances are required to get a good fit. Table 5 lists the resonances used in the final fits (column 1 and 2), their pole positions (column 3) and their decay modes leading to the $p\pi^0\eta$ final states (column 4). The fractional contributions (adding up to 100% of the integrated $p\pi^0\eta$ cross section) are listed in column 5, while

Table 3. Properties of the P_{33} K -matrix poles. The masses M_i and K -matrix coupling constants $g_\alpha^{(i)}$ from resonance (i) to the decay mode α are given in GeV, the helicities A in $\text{GeV}^{-\frac{1}{2}}$, s in GeV^2/c^4 ; the f - describing $N\pi \rightarrow \Delta\pi$ contact interactions - are dimensionless. The parameters marked with * were fixed in the fit.

		Pole 1	Pole 2	Pole 3	
	M_i	1232 \pm 3	1795 \pm 40	2020 \pm 80	
	$A_{1/2}$	-0.125	0.031	0.026	
	$A_{3/2}$	-0.264	0.123	0.081	
a		$g_a^{(1)}$	$g_a^{(2)}$	$g_a^{(3)}$	f_{1a}
1	$N(940)\pi$	1.20	1.25	0.92	-1.40
2	$\Delta(1232)\pi(P)$	-0.52	-1.73	-0.69	0.81
3	$\Delta(1232)\pi(F)$	0.*	0.19	-0.76	0.*
4	$\Delta(1232)\eta$	0.*	0.75	-0.63	0.*
5	$N(1535)\pi$	0.*	0.94	1.04	0.*
6	$N(940)\rho$	0.*	0.05	-0.06	0.*

Table 4. Properties of the D_{33} K -matrix poles.

		Pole 1	Pole 2	Pole 3	
	M_i	1780 \pm 50	1980 \pm 60	2400 \pm 90	
	$A_{1/2}$	+0.041	0.205	0.228	
	$A_{3/2}$	0.252	-0.003	0.143	
a		$g_a^{(1)}$	$g_a^{(2)}$	$g_a^{(3)}$	f_{1a}
1	$N(940)\pi$	0.31	0.66	1.22	-0.62
2	$\Delta(1232)\pi(S)$	0.51	-0.72	-0.16	-0.17
3	$\Delta(1232)\pi(D)$	-1.21	-1.49	-1.51	-0.63
4	$\Delta(1232)\eta$	-0.39	-0.23	0.81	0.*
5	$N(1535)\pi$	-0.38	-0.40	-0.78	0.*
6	$N(940)\rho$	-0.14	-0.26	-0.24	0.*

columns 6 and 7 give the likelihood change, for the total data set and for the data presented here, respectively, when a resonance is assumed not to couple to $p\pi^0\eta$.

In the P_{33} wave we find a first pole above $\Delta(1232)$ at $1510^{+20}_{-50} - i115 \pm 20\text{ MeV}/c^2$ and a further pole at $1980^{+25}_{-45} - i175^{+18}_{-28}\text{ MeV}/c^2$. If the couplings of the first pole to $p\pi\eta$ are reduced to zero, the likelihood for the $\gamma p \rightarrow p\pi\eta$ data deteriorates by 60. Removing $p\pi\eta$ couplings of the highest K-matrix pole ‘‘costs’’ 63 units in likelihood. If the latter pole is completely removed from the fit, the likelihood value for $\pi\eta$ channel changes by 177 and total likelihood by 2230. Such fits are unacceptable.

Using only $\Delta(1700)D_{33}$ for the D_{33} wave, no satisfactory description of the data was obtained; a second resonance proved to be essential. The pole position for the second resonance was found at $(1985 \pm 35) - i(195 \pm 25)\text{ MeV}/c^2$. The likelihood value for the $\gamma p \rightarrow p\pi^0\eta$ reac-

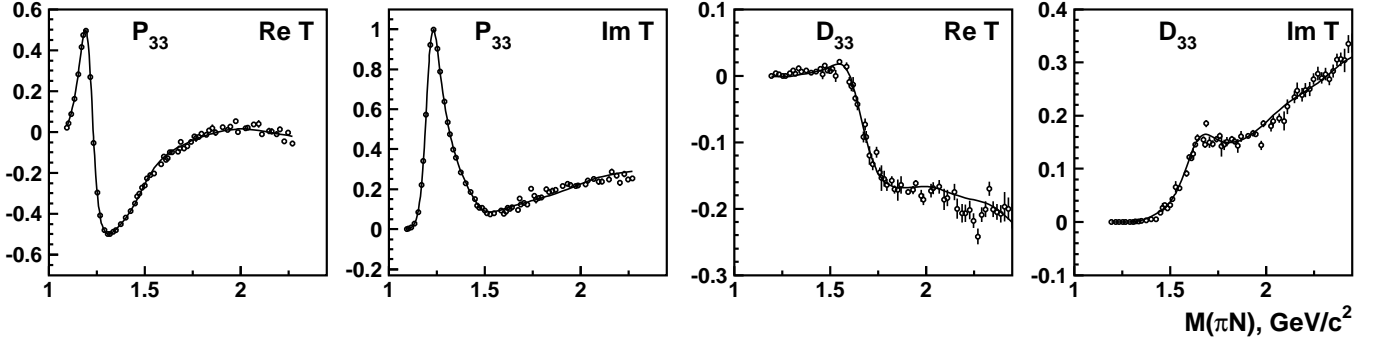


Fig. 8. The πN elastic scattering amplitude in the P_{33} (left) and D_{33} (right) wave [16] and our fit. The P_{33} shows the distinct phase motion for $\Delta(1232)$; a second resonance at $1600 \text{ MeV}/c^2$ is difficult to see, and there is no sign for a third resonance. Likewise, there is a rapid phase motion at $1700 \text{ MeV}/c^2$ in the D_{33} but no sign for any resonance above it.

Table 5. Resonances contributing to $\gamma p \rightarrow p\pi\eta$, their pole positions and decay modes, and change of likelihood when resonance couplings to $N\pi\eta$ are reduced to zero. A change in likelihood by 50 corresponds to a χ^2 change of 25 or to a statistical significance of 5σ .

Name	Wave	Pole (MeV/c^2)	Decay modes	Fraction	$\Delta \ln \mathcal{L}_{\text{tot}}$	$\Delta \ln \mathcal{L}_{\pi^0\eta}$
$N(1880)$	P_{11}	$1880 - i110$	$pa_0, N(1535)\pi$	12%	2050	70
$N(2200)$	P_{13}	$2200 - i150$	$pa_0, N(1535)\pi$	7%	1392	73
$\Delta(1600)$	P_{33}	$1510 - i115$	$\Delta\eta$	} 22%	884	60
$\Delta(1920)$	P_{33}	$1980 - i175$	$\Delta\eta, pa_0$		1818	63
$\Delta(1700)$	D_{33}	$1640 - i160$	$\Delta\eta, N(1535)\pi$	} 24%	2611	84
$\Delta(1940)$	D_{33}	$1985 - i195$	$\Delta\eta, pa_0, N(1535)$		1124	52
$\Delta(2360)$	D_{33}	$2320 - i250$	$\Delta\eta, pa_0, N(1535)$		1018	24
$\Delta(1905)$	F_{35}	$1920 - i145$	$\Delta\eta, N(1535)\pi$	7%	1991	65
t -channel ρ - ω -, u -channel p - Δ -exchange				28%	6340	208

tion changed by $\Delta \ln \mathcal{L}_{\gamma p \rightarrow p\pi^0\eta} = 151$, the total likelihood by 2005 units; these are highly significant numbers. With $\Delta(1940)D_{33}$ and without $\Delta(1700)D_{33}$, the fit was also unacceptable ($\Delta \ln \mathcal{L}_{\gamma p \rightarrow p\pi^0\eta} = 137$, $\Delta \ln \mathcal{L}_{\text{tot}} = 4782$). The fit improved notably ($\Delta \ln \mathcal{L}_{\gamma p \rightarrow p\pi^0\eta} = 28$, $\Delta \ln \mathcal{L}_{\text{tot}} = 770$) by adding a third D_{33} state. Its mass optimized at about $2.35 \text{ GeV}/c^2$ and a width in the $400\text{-}600 \text{ MeV}/c^2$ range. Its mass is close to the end of the available phase space. An upper bound for its mass is not well defined; hence we do not claim that this state exists.

When an additional $N(2000)D_{13}$ resonance decaying into $N(1535)\pi$ and $Na_0(980)$ was introduced, strong interference between the two amplitudes was observed which increases the systematical errors of the PWA results. A precise mass determination of the $\Delta(1940)D_{33}$ will hence require separation of the two isotopic resonances, e.g. by measurements of $\gamma N \rightarrow n\pi^+\eta$. This ambiguity affects of course the branching ratios as well.

We assign the absence of $\Delta(1920)P_{33}$ and $\Delta(1940)D_{33}$ in the phase shift analysis of Arndt *et al.* [16] to their weak couplings to the $N\pi$ channel. To check if our data are consistent with elastic scattering amplitudes, we included these amplitude in the fit. The result is shown in Fig. 8:

the existence of the two resonances is not in conflict with elastic scattering.

Fig. 3e shows a structure in the $p\pi^0$ invariant mass at about 1.5 GeV (while Fig. 3f would suggest a higher mass). We tested the possibility that the structure signals contributions from $\gamma p \rightarrow N(1520)\eta$ or $\gamma p \rightarrow \Delta(1600)\eta$. Both attempts yielded marginal improvements in likelihood and contributions of about 0.5%. The PWA interprets the structure as interference between $pa_0(980)$ and $N(1535)\pi$.

To check the stability of the solution we added, one by one, new resonances to the analysis. Adding a resonance with S_{31} or G_{37} quantum numbers returned masses at the end of the phase space, very broad widths, negligible fractional contributions and marginal improvements in likelihood. For a D_{35} wave, stable fit results were obtained with $M \approx 2150 \text{ MeV}$, $\Gamma \approx 160 \text{ MeV}$, and a 1% fractional contribution. The improvement of the likelihood was marginal, ≤ 10 . Adding a fourth pole to the D_{33} wave, reproduced the T-matrix pole position reported above and created an additional pole in the region of $2 \text{ GeV}/c^2$. However the statistical evidence for this was again marginal, likelihood changed by ≤ 10 . The present data do not support the need to introduce additional resonances. We tried

to improve the fits by adding decays of $\Delta(2360)D_{33}$ into $\Delta(1600)P_{33}\eta$ or $N(2200)P_{13} \rightarrow N(1710)\eta$. The statistical significance for these transition was weak, and the fractional contribution to the data stayed below 0.5%.

4.5 Scans

In a second analysis we replaced, alternatively, the P_{33} or D_{33} partial wave by a sum of a K-matrix for the energy region below $1.85 \text{ GeV}/c^2$ and a relativistic Breit-Wigner (BW) amplitude describing the higher-mass region. The mass of the P_{33} Breit-Wigner state was found to be $1995 \pm 50 \text{ MeV}$ and the width $380 \pm 60 \text{ MeV}$. The BW mass of the second D_{33} resonance was found to be $1970 \pm 50 \text{ MeV}$ and the width $350 \pm 70 \text{ MeV}$.

The findings can be visualized in scans showing the changes of $-\ln \mathcal{L}_{tot}$ obtained in the fit where the mass of a resonance under study is changed in steps and fixed while all other variables are allowed to vary freely. In Fig. 9, the P_{33} amplitude is described by three BW resonances, $\Delta(1232)$, $\Delta(1600)$ and a third resonance the mass of which is scanned. The mass of this third resonance was scanned from 1.85 to $2.5 \text{ GeV}/c^2$ and its width fixed to $350 \text{ MeV}/c^2$. Fig. 9 (left) shows the change in total likelihood, Fig. 9 (right) the likelihood chance for the data on $\gamma p \rightarrow p\pi^0\eta$. A clear minimum - which we identify with $\Delta(1920)P_{33}$ - is observed in both cases; the data on $\gamma p \rightarrow p\pi^0\eta$ have a preference for a somewhat higher mass.

In Fig. 10, a second D_{33} resonance is added to $\Delta(1700)$. Again, the mass scan covered the 1.85 to $2.5 \text{ GeV}/c^2$ region, and the width was fixed to $350 \text{ MeV}/c^2$. Wide minima are observed in the 1900 - $2020 \text{ MeV}/c^2$ region. The D_{33} wave shows a second minimum at about $2.4 \text{ GeV}/c^2$, in agreement with the fits described above. The first minimum is interpreted as evidence for $\Delta(1940)D_{33}$, the second one may indicate contributions from a higher mass resonance in this partial wave.

4.6 PWA results

Table 6 summarizes our results. The Breit-Wigner masses and widths and the pole positions are mostly compatible with Review of Particle Properties (RPP) [15]. Most decay branching ratios are reported here for the first time. They are calculated as ratio of partial decay width and total width at the position of the Breit-Wigner mass. The best known states in Table 6 are $\Delta(1600)P_{33}$, $\Delta(1700)D_{33}$, and $\Delta(1920)P_{33}$, all 3-star or 4-star resonances in [15]. The high rating does however not correspond to a good agreement in resonance properties derived in different analyses. In Table 7 we compare our pole positions with those of Höhler *et al.* [34], Cutkosky *et al.* [35], and Arndt *et al.* [16]. It is of course extremely intriguing that three out of five of them were not observed in the most recent analysis [16]. The $\Delta(1600)P_{33}$ K-matrix coupling to $\Delta\eta$ and $N(1535)\pi$ are sizable (see Table 3); when the pole is approximated by a Breit-Wigner resonance, its couplings to these two channels become very small due to phase space

Table 7. Pole positions (in MeV/c^2) of “well established” Δ resonances and the one-star $\Delta(1940)D_{33}$.

Resonance	Höhler	Cutkosky	Arndt	this work
$\Delta(1600)P_{33}$	1550	$1550 - i100$	$1457 - i200$	$1510 - i115$
$\Delta(1700)D_{33}$	$1651 - i80$	$1675 - i110$	$1632 - i126$	$1650 - i160$
$\Delta(1920)P_{33}$	1900	$1900 - i150$	not seen	$1980 - i155$
$\Delta(1905)F_{35}$	$1829 - i152$	$1830 - i140$	not seen	$1920 - i145$
$\Delta(1940)D_{33}$	not seen	$1900 - i100$	not seen	$1985 - i195$

limitations. The K-matrix pole and the Breit-Wigner mass differ considerably; this fact renders a definition of the helicity couplings difficult and we refrain from giving numbers.

The $\Delta(1920)P_{33}$ is the third resonance in this partial wave, after the well-known $\Delta(1232)$ and the Roper-like $\Delta(1600)P_{33}$. $\Delta(1920)P_{33}$ was observed in several analyses including those of Höhler *et al.* [34] and Cutkosky *et al.* [35] in elastic πN scattering data, and by Manley *et al.* [37] in a combined analysis of πN elastic scattering and pion induced double-pion production who found $M=2057 \pm 110$, $\Gamma=460 \pm 320 \text{ MeV}/c^2$. In RPP [15] it is ranked as 3-star resonance. In the analysis by Arndt *et al.* [16], $\Delta(1920)P_{33}$ was not found. $\Delta(1600)P_{33}$ is observed in all four analyses of Table 7; in [19], it was not needed to get a good description of the data taken into account at that time.

The $\Delta(1940)D_{33}$ state has only one star in the RPP classification. It was observed by Cutkosky *et al.* [35] in elastic πN scattering data with mass $M=1940 \pm 100 \text{ MeV}/c^2$ and width $\Gamma = 200 \pm 100 \text{ MeV}/c^2$, and by Chew *et al.* [36] at $M=2058 \pm 35 \text{ MeV}/c^2$ and $\Gamma=198 \pm 46 \text{ MeV}/c^2$ while Manley found $M=2071 \pm 100 \text{ MeV}/c^2$, $\Gamma=460 \pm 320 \text{ MeV}/c^2$ [37]. In [16], $\Delta(1940)D_{33}$ was not found.

The confirmation of the two resonances $\Delta(1920)P_{33}$ and $\Delta(1940)D_{33}$ in a new reaction is a major result of this analysis. In addition, several partial decay branching ratios have been determined. These provide first insight into an old question on how the mass of high-lying parent resonances is dissipated, into high-momenta of the daughter particles, into high-mass mesons or into high-mass daughter baryon resonances. The results suggest that high-mass parent baryons seem to take advantage of all allowed decay modes, including intermediate meson *and* baryon resonances even at rather high masses. The situation resembles $\bar{N}N$ annihilation [38,39]: in this process, the production of high-mass mesons is preferred in comparison to production of low-mass mesons even though the phase space is of course larger for the latter reaction. Likewise, there seems to be no preference for the kinematically favored $N\pi$ decay mode.

5 Summary and conclusions

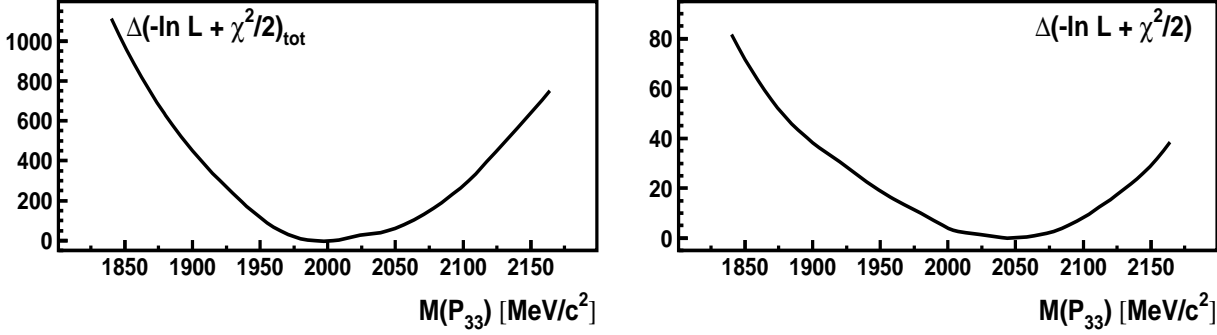


Fig. 9. Likelihood as a function of the mass of a ΔP_{33} resonance. The width is fixed to $350 \text{ MeV}/c^2$. The left plot gives the change of the total likelihood, the right plot the change of the likelihood contribution from $\gamma p \rightarrow p\pi^0\eta$, from this data and from beam asymmetry data [31]. The minimum (reference) value is at about $-280\,000$ (a) and $-6\,000$, respectively.

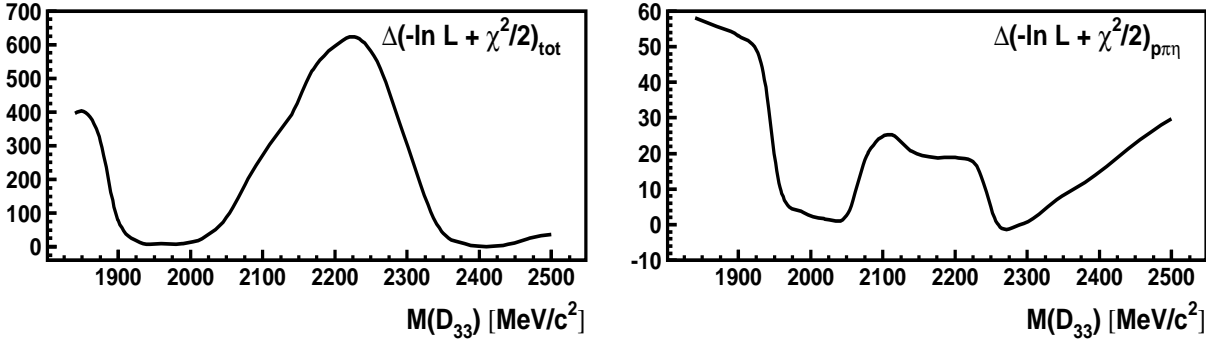


Fig. 10. Likelihood as a function of the mass of a ΔD_{33} resonance. The width is fixed to $350 \text{ MeV}/c^2$. The left plot gives the change of the total likelihood, the right plot the change of the likelihood contribution from $\gamma p \rightarrow p\pi^0\eta$, this data and beam asymmetry data [31].

Table 6. Pole positions, Breit-Wigner parameters, and decay branching ratios of Δ resonances. Masses and widths are given in MeV/c^2 , branching ratios in %. The branching ratios are corrected for Clebsch-Gordan coefficients and unseen decay modes of final-state mesons (π^0 and η). The helicity couplings are in $\text{GeV}^{-1/2}$.

	M_{pole}	Γ_{pole}	M_{BW}	Γ_{tot}^{BW}	$\text{Br}_{N\pi}$	$\text{Br}_{\Delta\eta}$	$\text{Br}_{N(1535)\pi}$	$\text{Br}_{Na_0(980)}$	$A_{1/2}$	$A_{3/2}$
$\Delta(1600)P_{33}$	1510^{+20}_{-50}	230 ± 40	1650 ± 40	530 ± 60	10 ± 3	0^a	0	0	not well defined	
$\Delta(1920)P_{33}$	1980^{+25}_{-45}	310^{+40}_{-60}	1990 ± 35	330 ± 60	15 ± 8	10 ± 5	6 ± 4	4 ± 2	22 ± 8	42 ± 12
$\Delta(1700)D_{33}$	1640 ± 25	325 ± 35	1790 ± 30	580 ± 60	20 ± 7	2 ± 1	4 ± 2	0	160 ± 40	150 ± 30
$\Delta(1940)D_{33}$	1985 ± 30	390 ± 50	1990 ± 40	410 ± 70	9 ± 4	4 ± 2	2 ± 1	2 ± 1	160 ± 40	110 ± 30
$\Delta(2360)D_{33}$	2320 ± 60	500 ± 100	2310 ± 60	640 ± 120	10 ± 4	60 ± 20	7 ± 4	9 ± 4	≈ 20	≈ 40

^a The partial width at the Breit-Wigner mass vanishes due to phase space arguments. The integrated contribution is in the order of a few %.

We have reported a study of the photoproduction process $\gamma p \rightarrow p\pi^0\eta$ at the Electron Stretcher Apparatus ELSA at Bonn. About 16000 $p\pi^0\eta$ events were extracted above a small background. For small photon energies, the cross section for the reaction agrees with previous results from Sendai and Graal. In this energy region, the process is dominated by the $\Delta(1232)\eta$. At higher photon energies, a significant fraction of the process proceeds via the $N(1535)\eta$ and some $pa_0(980)$ contribution is observed.

A partial wave analysis determines the resonant contributions. Two waves with P_{33} and D_{33} quantum numbers, with $J^P = 3/2^+$ and $3/2^-$, dominate the reaction. We find evidence for two resonances $\Delta(1920)P_{33}$ and $\Delta(1940)D_{33}$ and indications for a further high-mass D_{33} resonance. The evidence for the two states was already communicated in a letter publication [40].

A detailed discussion of the role of $\Delta(1920)P_{33}$ and $\Delta(1940)D_{33}$ within the spectrum of Δ resonances will be

given elsewhere [41]. Here we just mention the main results.

1. In [41], the 3 negative parity resonances $\Delta(1900)S_{31}$, $\Delta(1940)D_{33}$, and $\Delta(1930)D_{35}$ are interpreted as triplet of resonances with $L = 1, S = 3/2, N = 1$ coupling to $J = 1/2, 3/2, 5/2$ and belonging to the $(D, L_N^P) S = (56, 1_3^-) 3/2$ supermultiplet. Alternatively, $\Delta(1900)S_{31}$ and $\Delta(1940)D_{33}$ could be a $L = 1, S = 1/2, N = 1$ doublet, and $\Delta(1930)D_{35}$ and $\Delta(2200)G_{37}$ a $L = 3, S = 1/2$ doublet. The mass of the triplet is rather low compared to quark model predictions [1, 2] while the $\Delta(2200)G_{37}$ mass is perfectly compatible with the models.
2. The two resonances $\Delta(1920)P_{33}$ and $\Delta(1940)D_{33}$ form a parity doublet [42]. Parity doublets are of topical interests, we refer the reader to two recent reviews [44, 45]. In the latter review, there is a written request to search for the doublet reported here. The conjecture that the reason for the mass degeneracy is due to a restoration of chiral symmetry in high-mass baryon states falls of course outside of experimental observability, and the interpretation is controversially discussed [46, 47, 48].
3. All masses in the Δ spectrum are perfectly compatible with models based on AdS/QCD when confinement is modeled by a soft wall in the holographic variable [12]. The hard wall approximation [11] gives a good general survey but fails in important details.

Acknowledgement

We would like to thank the technical staff of ELSA and of the participating institutions for their invaluable contributions to the success of the experiment. We acknowledge financial support from the Deutsche Forschungsgemeinschaft (DFG-TR16) and the Schweizerische Nationalfond. The collaboration with St. Petersburg received funds from DFG and RFBR. This work comprises part of the thesis of I. Horn.

References

1. S. Capstick, N. Isgur, Phys. Rev. D **34** (1986) 2809.
2. U. Löring, B. C. Metsch and H. R. Petry, Eur. Phys. J. A **10** (2001) 395, 447.
3. L. Y. Glozman, W. Plessas, K. Varga and R. F. Wagenbrunn, Phys. Rev. D **58** (1998) 094030.
4. M. Anselmino, E. Predazzi, S. Ekelin, S. Fredriksson and D.B. Lichtenberg, Rev. Mod. Phys. **65** (1993) 1199.
5. M. Kirchbach, M. Moshinsky and Yu. F. Smirnov, Phys. Rev. D **64** (2001) 114005.
6. E. Santopinto, Phys. Rev. C **72** (2005) 022201.
7. J. M. Maldacena, Adv. Theor. Math. Phys. **2** (1998) 231 [Int. J. Theor. Phys. **38** (1999) 1113].
8. E. Witten, Adv. Theor. Math. Phys. **2** (1998) 253.
9. I.R. Klebanov, arXiv:hep-th/0009139.
10. A. Karch, E. Katz, D. T. Son and M. A. Stephanov, Phys. Rev. D **74** (2006) 015005.
11. S.J. Brodsky, Eur. Phys. J. A **31** (2007) 638.
12. H. Forkel, M. Beyer and T. Frederico, JHEP **0707** (2007) 077.
13. H. Forkel, M. Beyer and T. Frederico, Int. J. Mod. Phys. E **16** (2007) 2794.
14. S. Basak *et al.*, Phys. Rev. D **76** (2007) 074504.
15. W.M. Yao *et al.*, J. Phys. G **33** (2006) 1 and 2007 partial update for the 2008 edition.
16. R. A. Arndt, W.J. Briscoe, I.I. Strakovsky and R.L. Workman, Phys. Rev. C **74** (2006) 045205.
17. B. Metsch, private communication, 2007.
18. A. V. Anisovich, A. Sarantsev, O. Bartholomy, E. Klempt, V. A. Nikonov and U. Thoma, Eur. Phys. J. A **25** (2005) 427.
19. A. V. Sarantsev, V. A. Nikonov, A. V. Anisovich, E. Klempt and U. Thoma, Eur. Phys. J. A **25** (2005) 441.
20. B.M.K. Nefkens, PiN Newslett. **13** (1997) 270.
21. J. Ajaka *et al.*, Phys. Rev. Lett. **100** (2008) 052003.
22. W. Hillert, Eur. Phys. J. A **28S1** (2006) 139.
23. E. Aker *et al.*, Nucl. Instrum. Meth. A **321** (1992) 69.
24. U. Thoma *et al.*, Phys. Lett. B **659** (2008) 87.
25. H. van Pee *et al.* [CB-ELSA Collaboration], Eur. Phys. J. A **31** (2007) 61 [arXiv:0704.1776 [nucl-ex]].
26. G. Suft *et al.*, Nucl. Instrum. Meth. A **538** (2005) 416.
27. A.V. Anisovich, E. Klempt, A.V. Sarantsev and U. Thoma, Eur. Phys. J. A **24** (2005) 111.
28. A.V. Anisovich and A.V. Sarantsev, Eur. Phys. J. A **30** (2006) 427.
29. A.V. Anisovich, V.V. Anisovich, E. Klempt, V.A. Nikonov and A.V. Sarantsev, Eur. Phys. J. A **34** (2007) 129152.
30. A.V. Anisovich, V. Kleber, E. Klempt, V.A. Nikonov, A.V. Sarantsev and U. Thoma, Eur. Phys. J. A **34** (2007) 243.
31. E. Gutz *et al.*, “The photon beam asymmetry for the reaction $\gamma p \rightarrow p\pi^0\eta$ ”, in preparation.
32. E. Gutz *et al.*, Eur. Phys. J. A **35** (2008) 291.
33. T. Nakabayashi *et al.*, Phys. Rev. C **74** (2006) 035202.
34. G. Höhler, F. Kaiser, R. Koch and E. Pietarinen, “Handbook Of Pion Nucleon Scattering,” Published by Fachinform. Zentr. Karlsruhe 1979, 440 P. (Physics Data, No.12-1 (1979)).
35. R.E. Cutkosky, C.P. Forsyth, J.B. Babcock, R.L. Kelly and R.E. Hendrick, “Pion - Nucleon Partial Wave Analysis,” 4th Int. Conf. on Baryon Resonances, Toronto, Canada, July 14-16, 1980. QCD161:C45:1980.
36. D.M. Chew, “New Δ Parameters From A Simpler, Cheaper And More Reliable πN Partial Wave Analysis”, 4th Int. Conf. on Baryon Resonances, Toronto, Canada, July 14-16, 1980. QCD161:C45:1980.
37. D.M. Manley, E.M. Saleski, Phys. Rev. D **45** (1992) 4002.
38. J. Vandermeulen, Z. Phys. C **37** (1988) 563.
39. E. Klempt, C. Batty and J.M. Richard, Phys. Rept. **413** (2005) 197.
40. I. Horn *et al.*, “Evidence for a parity doublet $\Delta(1920)P_{33}$ and $\Delta(1940)D_{33}$ from $\gamma p \rightarrow p\pi^0\eta$ ”, submitted to PRL.
41. E. Klempt, “ Δ resonances: quark models, chiral symmetry and AdS/QCD”, accompanying paper.
42. L.Y. Glozman, Phys. Lett. B **475** (2000) 329.
43. T. D. Cohen and L. Y. Glozman, Phys. Rev. D **65** (2002) 016006 [arXiv:hep-ph/0102206].

44. R.L. Jaffe, D. Pirjol and A. Scardicchio, Phys. Rept. **435** (2006) 157.
45. See, e.g., L.Y. Glozman, Phys. Rev. Lett. **99** (2007) 191602, and references therein.
46. E. Klempt, Phys. Lett. B **559** (2003) 144.
47. E. Klempt and A. Zaitsev, Phys. Rept. **454** (2007) 1.
48. M. Shifman and A. Vainshtein, PR D **77** (2008) 034002.